GaAs multilayer p^+-i homojunction far-infrared detectors

A. G. U. Perera,[a] H. X. Yuan, S. K. Gamage, W. Z. Shen, and M. H. Francombe
Department of Physics and Astronomy, Georgia State University, Atlanta, Georgia 30303

H. C. Liu and M. Buchanan
Institute for Microstructural Sciences, National Research Council, Ottawa K1A 0R6, Canada

W. J. Schaff
School of Electrical Engineering, Cornell University, Ithaca, New York 14853

(Received 28 June 1996; accepted for publication 27 December 1996)

A molecular beam epitaxy grown wavelength tunable GaAs p^+-i homojunction interfacial work-function internal photoemission far-infrared detector is developed. The multilayer (p^+-i-p^+-i-...) detector structures consist of 2, 5, and 10 emitter layers. Experimental results are explained in terms of the number of emitter layers and the doping concentrations of the emitter layer. A detector with 10 multilayers and an emitter layer doping concentration (N_e) of 3×10^{18} cm^{-3} shows a current responsivity of 2 A/W, an effective quantum efficiency of 9.2% (at 26.3 μm) with a cutoff wavelength of 85 μm and the noise equivalent power of 2.18×10^{-12} W/$\sqrt{\text{Hz}}$ at 4.2 K. © *1997 American Institute of Physics.* [S0021-8979(97)03207-6]

I. INTRODUCTION

During recent years, considerable interest has arisen in the development of internal-photoemission semiconductor-junction structures for the detection of IR photons. Various formats and modes of operation have been considered.[1–3] It was shown[1] using commercial Si p-i-n diodes at 4.2 K, that an interfacial work-function (IWF) (Δ), which determines the detection cutoff wavelength defined as $\lambda_c=\lambda_t$ (threshold) $=1.24/\Delta$ for internal photoemission, exists at the interface and can be varied by varying the emitter (n^+ or p^+) layer doping concentration (N_e). Perera *et al.*[4] demonstrated much longer λ_c's for Si (220 μm), Ge (240 μm), and InGaAs (90 μm), again on p-i-n diodes.

Recent modeling studies[2,5] found that high performance, wavelength tunable FIR detectors could be realized if the emitter layer is doped above the metal-insulator (M-I) transition value but below the critical value at which Δ just vanishes. These types of detectors are labeled homojunction interfacial work-function internal photoemission (HIWIP) detectors.[2] The basic structure of a single layer HIWIP detector consists of a highly doped emitter/absorber layer, an intrinsic layer, and a highly doped collector layer. Fig. 1(a) shows the energy-band diagrams of a multilayer (p^+-i-p^+-i...) structure under forward bias. The IWF, $\Delta=\Delta E_v-E_F$, with ΔE_v being the major band edge offset due to the band-gap narrowing effect[2] and E_F the Fermi energy relative to the major band edge. A relationship between Δ (λ_c) and N_e has been obtained based on the high-density (HD) theory.[2]

The total quantum efficiency (η) model[2] for Si can be used for GaAs with trivial modifications. For high internal quantum efficiency, a thin emitter layer is needed so that photoexcited carriers can be collected. The optimum emitter layer thickness (W_e) results from the tradeoff of photon absorption and hot electron scattering.[2] To reduce undesired modifications to barrier shape caused by the space-charge effect, a thin i layer with a low compensating impurity concentration is required.[5] However, a too thin W_i will lead to increased direct tunneling which will dominate the dark current. The η could be further increased using multilayer structures, due to the increased photon absorption efficiency and possible photocurrent gain enhancement.[2] Calculations[2] have shown that Si HIWIP FIR detectors could have a performance comparable to that of conventional Ge FIR photoconductors[6] or Ge blocked-impurity-band (BIB) FIR detectors,[7] and with unique material advantages. It is noted that the photodetection mechanism of HIWIP detectors is similar to that of other types of internal photoemission detectors,[8] such as the Schottky barrier (3–5 μm) and the $Si_{1-x}Ge_x$/Si detectors (8–14 μm). A stacked SiGe/Si HIP multilayer detector was also demonstrated,[3] showing enhanced photoresponse.

In addition to n- and p-Si, significant effective band-gap shrinkage has also been observed for heavily doped p-GaAs.[9] Better carrier transport properties of GaAs, such as higher mobility will translate into a higher gain, which may produce improved performance for this type of detector. Also, the recent rapid development of GaAs based long-wavelength quantum-well focal plane array cameras make GaAs another promising candidate for developing HIWIP FIR detectors. The progress[6] of n-GaAs FIR photoconductors has been slow due to difficulties in growing high purity materials. Here we report for the first time the development of GaAs multilayer p-i HIWIP FIR detectors. The p-type dopant is Be which has an ionization energy of 28 meV in p-GaAs, and the residual impurity concentration in the i layer is dominated by acceptors.

II. EXPERIMENTAL DETAILS

Four multilayer structures were designed as shown in Fig. 1(b), with the device parameters listed in Table I. The wafers were grown by MBE technology at a substrate temperature of 560 °C. A 4000 Å bottom contact (p^{++}) layer was first grown on the undoped GaAs substrate, followed by a 1500 Å undoped (i) layer. Then 2–10 periods of thin emitter (p^+) layers (W_e=150–300 Å) and i layers

[a]Electronic mail: phyuup@panther.gsu.edu

 0021-8979/97/81(7)/3316/4/$10.00

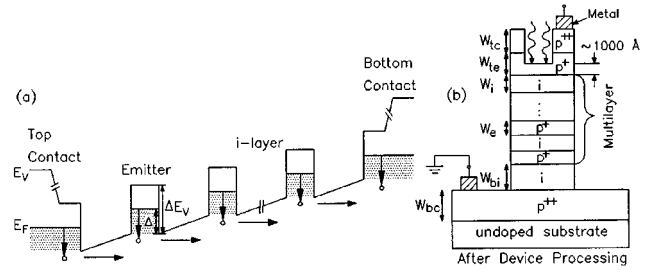

FIG. 1. (a) Energy-band diagram of a multilayer HIWIP detector under forward bias. Here, ΔE_v is the valence-band-edge offset at the p^+-i interface due to the band-gap narrowing effect, Δ the interfacial workfunction, and E_F the Fermi level relative to the valence-band edge. (b) Schematic structure of the multilayer HIWIP detector. p^{++} is the contact layer, p^+ the emitter layer, and i the undoped layer. A window is opened on the top side for frontside illumination.

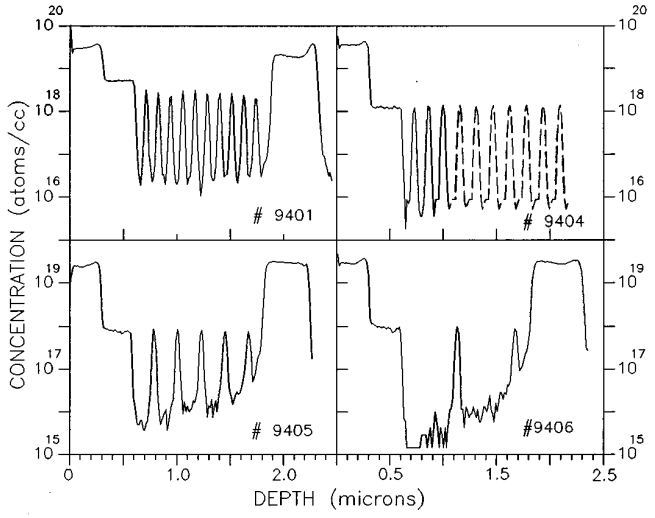

FIG. 2. SIMS profiles of our four Be-doped p-GaAs HIWIP detector samples. The measurement for No. 9404 is not complete and the dashed curve is the extrapolation. The background concentration of As is 10^5 atoms/cm^3 in all four samples.

(W_i=1000–5000 Å) were grown, followed by a 3000 Å top emitter layer and a 3000 Å top contact layer. The top and bottom contact layers were doped to $(2–4)\times10^{19}$ cm^{-3}, far above the metal-insulator (Mott) transition value to ensure an ohmic contact. The emitter layers were doped to $(1-3)\times10^{18}$ cm^{-3}. An optical window was opened on the top by etching, for frontside illuminated operation. The thickness of the top emitter layer within the window is kept around 1000 Å to reduce undesired photon absorption loss. Mesa elements with various areas (from 400×400 to 800×800 μm^2) were delineated by wet etching techniques. The contact was formed by deposition of Ti-Pt-Au. Secondary-ion-mass spectroscopy (SIMS) measurements as evident from Fig. 2 show that the background acceptor concentrations are around 2×10^{16} cm^{-3} for No. 9401, $(2–4)\times10^{15}$ cm^{-3} for No. 9404, $(4–5)\times10^{15}$ cm^{-3} for No. 9405, and $(2–4)\times10^{15}$ cm^{-3} for No. 9406.

III. RESULTS AND DISCUSSION

Spectra were taken with a Perkin–Elmer system 2000 FTIR spectrometer, with the samples mounted in a HD-3L dewar with a 15 μm cut-on cold filter. A Si bolometer was used as the reference detector to obtain the background spectrum and the responsivity. The bolometer, which has a flat response up to ~1 mm was calibrated using the load curve[10] and found to be $[3.4\pm0.03]\times10^5$ A/W, in excellent agreement with the responsivity given by the manufacturer (3.4×10^5). Fig. 3 shows the spectral responses measured at different forward biases for two samples of No. 9401 and No. 9404. The long tailing behavior in the long wavelength region reflects the nature of internal photoemission. The wavelength where the spectrum signal first reaches zero is at 92 ± 1 μm for No. 9401 and 83 ± 1 μm for No. 9404, corresponding to the Δs of $13.5^{+0.2}_{-0.1}$ meV and $14.9^{+0.2}_{-0.1}$ meV, respectively. The wavelength at which the mean (of at least 8 curves) response first reaches the same level as the maximum of the standard deviation of the spectra, (i.e., noise level), which we denote as λ_c, is 85 ± 1 μm for No. 9401 (at 193 mV bias) and 76 ± 1 μm for No. 9404 (at 91.5 mV bias) as determined in Fig. 4. The inset in Fig. 3 (a) show an Arrhenius plot (of dark current versus reciprocal temperature,) for No. 9401 resulting in a Δ of 11.6 ± 0.4 meV at 12 mV bias (labeled 2) indicating λ_c is even longer than 92 μm. The discrepancy results mainly from the energy loss of the photoexcited carriers by inelastic scattering prior to the carrier emission. For 6 mV bias (labeled 1) it is 11.2 ± 0.4 meV. The longer λ_c is reasonable since the experimental determination

TABLE I. Parameters for four detector structures. Measured (from spectrum) interfacial work-function (Δ),[a] peak quantum efficiency η_p, NEP and calculated Fermi level from HD theory (E_F). The valence-band-edge offset is given by $\Delta E_v=\Delta+E_F$. Here, W_i, W_e, and W_{bi} are the thicknesses of the intrinsic (i), emitter (p^+), and bottom intrinsic (i), respectively. N_e and N_c are the doping concentrations of the emitter and contact layers, respectively. The thickness of the top contact (p^{++}), the top emitter (p^+) and bottom contact (p^{++}) layers, W_{tc}, W_{te} and W_{bc} were 3000, 3000, and 4000 Å, respectively, for four samples.

Sample No.	Number of layer	W_i (Å)	W_e (Å)	N_e (cm^{-3})	W_{bi} (Å)	N_c (cm^{-3})	Δ (meV)	E_F (meV)	ΔE_v (meV)	η_p %	NEP (10^{-12}W/$\sqrt{\text{Hz}}$)
9401	10	1000	150	3×10^{18}	1500	$(2–3)\times10^{19}$	$14.6^{+0.1}_{-0.2}$	10.2	25.0	9.2	2.18
9404	10	1000	300	1×10^{18}	1500	$(3–4)\times10^{19}$	$16.8^{+0.2}_{-0.3}$	4.9	21.7	4.8	2.77
9405	5	2000	300	1×10^{18}	1500	$(2–3)\times10^{19}$	~17.0	4.9	21.9	5.7	3.76
9406	2	5000	300	1×10^{18}	1500	$(3–4)\times10^{19}$	~17.0	4.9	21.9	2.5	11.50

[a]Δ's for two samples, No. 9405 and No. 9406, are rough estimates, since the corresponding spectra are very noisy.

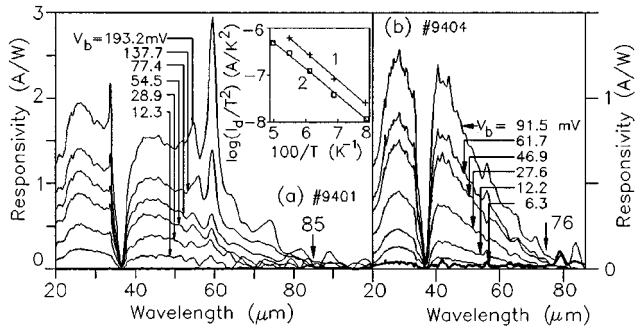

FIG. 3. Spectral response measured at 4.2 K for two samples at different forward biases: (a) No. 9401 with $N_e=3\times10^{18}$ cm^{-3}, showing a cutoff of 85 ± 1 μm. The deep valley at 36.5 μm is due to the transverse optical (TO) phonons of GaAs, and the spike at 59.5 μm is mainly associated with the defects in the surface or interfaces of the sample. The inset in (a) shows an Arrhenius plot for No. 9401 indicating a Δ of 11.6 ± 0.4 meV at 12 mV (labeled as 2) and 11.2 ± 0.4 meV at 6 mV (labeled as 1) corresponding to an even longer λ_c. (b) No. 9404 with $N_e=1\times10^{18}$ cm^{-3}, showing a cutoff of 76 ± 1 μm.

of zero response is determined by the noise as shown in Fig. 4. The responsivity curves show a strong bias dependence, increasing significantly with increasing bias. However, the bias cannot be increased indefinitely as the dark current also increases with bias.[2] The λ_c also shows a strong bias dependence in the low bias range as seen in Si HIWIP modeling.[2] The spectral response at reverse biases is similar to that at forward biases, but the responsivity is somewhat smaller as expected since the top emitter has no contribution to photocurrent for the reverse bias case.

It is noted that the spectral response exhibits a deep valley between 35 and 40 μm. The valley minima are at 36.5 μm (34.0 meV) for No. 9401 and 36.6 μm (33.9 meV) for No. 9404 corresponding to the transverse optical phonon energy in GaAs.[11] The peak near 35 μm associated with the absorption minima at 36 μm is a characteristic feature of GaAs absorption and reflection curves.[11] The sample No. 9401 exhibits a remarkably reproducible spike response at 59.5 μm, which is not due to noise as is evident from Fig. 4. This becomes stronger with increasing bias as shown in Fig. 3(a). It mainly has two origins: one is due to the phonon

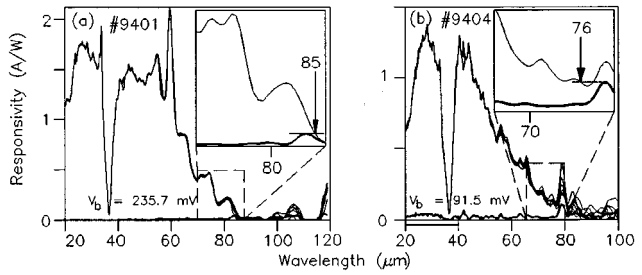

FIG. 4. (a) Spectral response for No. 9401 taken at 235.7 mV repeated for 8 times over a period of 5 h. The peak at around 60 μm exhibit excellent overlap in the 8 curves as seen, confirming that it could not be due to noise. The dark line indicate the deviation (noise level) curve. (b) The spectral response for No. 9404 taken at 91.5 mV repeated for 16 times over a period of 10 h, with the standard deviation (dark curve). The insets in (a) and (b) are the blow ups of the marked area of the mean and the deviation curves to show the determination of λ_c.

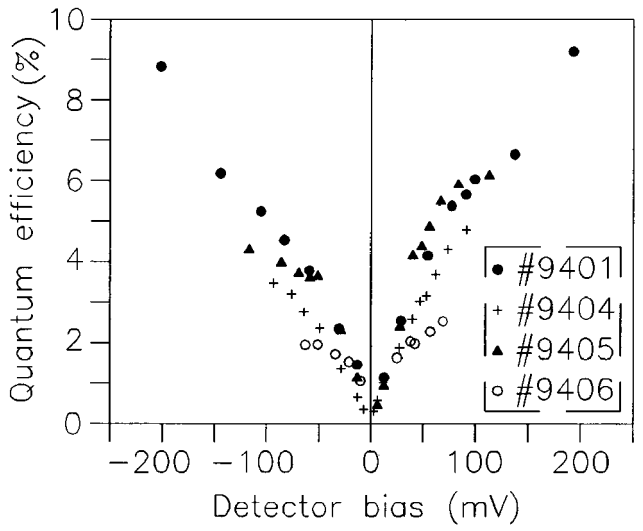

FIG. 5. Bias dependence of effective peak quantum efficiency (η_p) measured for No. 9401 (10-layer), No. 9404 (10-layer), No. 9405 (5-layer), and No. 9406 (2-layer). The λ_p is 26.3 μm for No. 9401 and 28.3 μm for No. 9404. The η_p's of No. 9405 and No. 9406 are measured at the wavelength equal to the λ_p of No. 9404.

vibrations and the other is due to the defects in the sample. Our experimental results show that it almost disappears in lower doped emitter layer samples [see Fig. 3(b)] and its position also changes with different doping concentrations. This indicates that it is mainly associated with the defects in the surface or interfaces of the sample. It is expected that with the further increase of N_e, the effective spectral response could be moved to a much longer wavelength range far beyond the phonon wavelength, as shown by our previous modeling work.[2]

The apparent peak wavelength (λ_p) and peak responsivity (R_p) can be obtained from Fig. 3, even though their real values may be hidden by the phonon-induced deep valley, resulting in smaller apparent values for both R_p and λ_p. We can see that λ_p is independent of bias. The bias dependence of apparent peak quantum efficiency ($\eta_p=R_p/0.806\lambda_p$) for the four samples is plotted in Fig. 5 for both forward and reverse cases. Based on bolometer uncertainties, the uncertainty in R_p is around 0.8%. For No. 9401, $\eta_p=9.2\%$ at 193.2 mV, with $\lambda_p=26.3$ μm. For No. 9404, $\eta_p=4.8\%$ at 91.5 mV, with $\lambda_p=28.3$ μm. The obtained η is higher than the expected value for a single layer detector and the η of the 2-layer sample is less than those of 5-layer and 10-layer samples, demonstrating the quantum efficiency enhancement due to multilayers. It is also noted that the measured η of the 5-layer sample is even larger than that of the 10-layer sample. One possibility is due to the difference in the window/mesa size (260/400 μm for 5-layer and 620/800 μm for 10-layer) and the assumption of uniform incident light density used in the data analysis. A nonuniform light density over the larger mesa area will reduce the effective η. Another possibility is that if the total emitter layer thickness is approaching the effective photon absorption length, further increasing the number of layers will no longer increase the absorption efficiency, while possible trapping effects may decrease the photo-carrier collection efficiency.

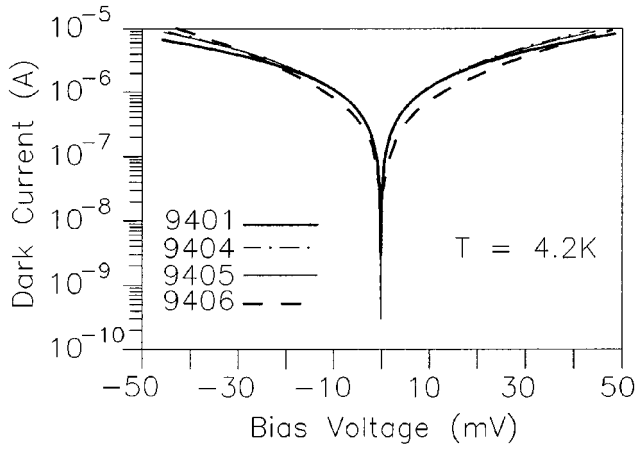

FIG. 6. Dark current-voltage characteristics for the four detectors at 4.2 K. The dark current at zero bias is 2.95×10^{-9} A, 6.03×10^{-10} A, 3.02×10^{-10} A, and 9.43×10^{-8} A for No. 9401, No. 9404, No. 9405, and No. 9406, respectively. Note that three curves for No. 9401, No. 9404 and No. 9405 almost coincide at low biases.

The net result is a reduction of effective η. The strong bias dependence of η results from the image-force and space-charge effects,[2,5] due to which the interfacial barrier maximum moves toward the emitter interface with increasing bias; hence the barrier collection efficiency increases. These effects also result in a voltage-tunable λ_c by lowering the barrier height with increasing bias. It is seen that η_p increases monotonically with increasing bias. For the same bias value, the forward η_p is larger than the reverse η_p, indicating the difference of absorption efficiency between the two cases. In addition, at the same bias, the sample with a higher N_e value shows a higher η value, which is due to the increase in absorption efficiency.

Another two important parameters for the detectors are the noise equivalent power (NEP) and the dark current. Fig. 6 shows the dark current-voltage characteristics at 4.2 K for the four HIWIP detectors. The relatively high dark current in No. 9401 detector at zero bias is due to its high doping concentration of the emitter layers, while the much higher dark current in No. 9406 detector at zero bias is probably due to the severe edge leakage, resulting in poor photoresponse. Using the measured peak responsivity and the dark current data, we can estimate the NEP of our GaAs HIWIP FIR detectors. The estimated peak NEP values at 4.2 K and near 50 mV forward bias are 2.18×10^{-12} W/$\sqrt{\text{Hz}}$ for No. 9401, 2.77×10^{-12} W/$\sqrt{\text{Hz}}$ for No. 9404, 3.76×10^{-12} W/$\sqrt{\text{Hz}}$ for No. 9405, and 1.15×10^{-11} W/$\sqrt{\text{Hz}}$ for No. 9406. We can see that the NEP value decreases with increasing doping concentration and multilayer number due to the increase of absorption efficiency and multilayer effect described above.

Up to now, there are no experimental data available for the band-edge shifts in any heavily doped semiconductors due to band-gap narrowing (BGN) effect, even though the total BGN value, which includes the shifts of both conduction and valence band edges ($\Delta E_g=\Delta E_c+\Delta E_v$), could be obtained by the optical[12] and electrical[9] measurements. Based on the measured value of Δ, the major band edge offset at the p^+-i interface can be estimated by $\Delta E_v=\Delta+E_F$. The Fermi energy can be calculated using the high-density theory.[2] The values of Δ, E_F, and ΔE_v are given in Table I. By combining ΔE_v with ΔE_g measured with other techniques, the minor band edge offset can be obtained, $\Delta E_c=\Delta E_g-\Delta E_v$. It was shown that the calculated E_F values in p-type semiconductors are larger than the actual values (especially for very high doping concentrations) which can be measured by the low temperature photoluminescence (PL) spectroscopy.[12] Therefore, it is expected that many important properties of heavily doped semiconductors, such as ΔE_g, E_F, ΔE_v, and ΔE_c, could be obtained by combining measurements of PL structures and HIWIP detectors. One of the goals of our work is to fabricate and measure various detector samples with different emitter layer doping concentrations to obtain the Δ–N_e relationship in a wide range, which is essential for the design of HIWIP detectors.

IV. CONCLUSION

In summary, we have demonstrated for the first time the HIWIP concept using MBE grown GaAs p^+-i multilayer structures. The test samples show high photoresponse due to multilayer enhancement. The cutoff wavelength is tunable by changing emitter layer doping concentration (λ_c increases from 76 to 85 μm as N_e increases from 1 to 3×10^{18} cm^{-3}), and is also voltage tunable. The NEP of the detectors has also been estimated to be of the order of 10^{-12} W/$\sqrt{\text{Hz}}$. Preliminary results obtained are promising and show that p-GaAs HIWIP detectors have great potential to become a strong competitor in FIR applications. Based on these results, it is possible to design detectors with wider wavelength ranges or to have multicolor detectors by changing the adjacent emitter layer doping concentrations.

ACKNOWLEDGMENTS

This work was supported in part by the National Science Foundation under grant No. ECS-94-12248. The authors acknowledge P. Chow-Chong and P. Marshall for sample fabrication and S. Rolfe for SIMS measurements.

[1] D. D. Coon, R. P. Devaty, A. G. U. Perera, and R. E. Sherriff, Appl. Phys. Lett. **55**, 1738 (1989).
[2] A. G. U. Perera, in *Physics of Thin Films*, edited by M. H. Francombe and J. L. Vossen (Academic, New York, 1995), Vol. 21, pp. 1–75.
[3] J. S. Park, T. L. Lin, E. W. Jones, H. M. Del Castillo, and S. D. Gunapala, Appl. Phys. Lett. **64**, 2370 (1994).
[4] A. G. U. Perera, R. E. Sherriff, M. H. Francombe, and R. P. Devaty, Appl. Phys. Lett. **60**, 3168 (1992).
[5] H. X. Yuan and A. G. U. Perera, J. Appl. Phys. **79**, 4418 (1996).
[6] E. E. Haller, Infrared Phys. **35**, 127 (1994).
[7] D. M. Watson, M. T. Guptill, J. E. Huffman, T. N. Krabach, S. N. Raines, and S. Satyapal, J. Appl. Phys. **74**, 4199 (1993).
[8] F. D. Sheperd, Proc. SPIE **1735**, 250 (1992).
[9] E. S. Harmon, M. R. Melloch, and M. S. Lundstrom, Appl. Phys. Lett. **64**, 502 (1994).
[10] F. J. Low, J. Opt. Soc. Am. **51**, 1300 (1961).
[11] E. D. Palik and R. T. Holm, in *Nondestructive Evaluation of Semiconductor Material and Devices*, edited by J. N. Zemel (Plenum, New York, 1979), pp. 315–395.
[12] D. Olego and M. Cardona, Phys. Rev. B **22**, 886 (1980).